Modelling of dune patterns by short range interactions

Clément Narteau, Eric Lajeunesse, François Métivier & Olivier Rozier
Equipe de Géomorphologie, Laboratoire de Dynamique des Systèmes Géologiques,
Institut de Physique du Globe de Paris, 75252 Paris cedex 05, France (narteau@ipgp.jussieu.fr).

A $3D$ cellular automaton is disclosed that enables modelling the dynamics of bedform. The overall mechanism can be regarded as a Markov chain, a discrete system with a finite number of configurations and probabilities of transition between them. Physical processes such as erosion, deposition and transport are modelled at the elementary scale by nearest neighbour interactions. At larger length scales, topographic structures arise from internal relationships based upon these short range interactions. This article focuses on crescentic barchan dunes that are used as a benchmark for our numerical model of bedforms. Length and time scales of isolated barchan dunes are studied in order to constrain the parameters of the model. Then we discuss pattern selection and the evolution of a population of dunes over a wide range of initial and boundary conditions. We eventually show that our model can be generalized to bedforms through the increase of the sand availability.

1 Introduction

There is a considerable variation within bedforms as they locally depend on the topography, the sediment load, and the flow. Such variability might be expressed by different relationships between erosion and deposition rates and the fluid velocity field. While empirical relationships estimate these quantities for a given bed under particular conditions, theoretical relationships simplify the turbulence problem to make easier the description of the sediment capacity of the flow. In both cases, it remains extremely difficult to tackle the impact of the size distribution of sediment particles. Despite these limitations, the study of aeolian dunes has significantly filled the gap between observations and models (Bagnold 1941; Pye and Tsoar 1990; Lancaster 1995).

Under dry conditions, the transport of sand grains by the wind involves similar physical mechanisms than sediment transport in liquids. However the absence of cohesion, dissolution and sedimentation limits the number of relations between fluid and solid ingredients. Then, in order to investigate couplings between wind and topography, it is sufficient to formalize the wind velocity field with respect to the surface profile as well as the erosion and deposition responses to shear stress (Jackson and Hunt 1975; Hunt et al. 1988; Weng et al. 1991). In this framework, the principle of mass conservation is commonly ensured by a continuity equation for the height profile

$$\partial_t h \; = \; - \, \partial_x q \tag{1}$$

where q is defined as a volumic sand flux per unit of time and per unit of length perpendicularly to the wind direction. The capacity of transport takes therefore the form of a saturated sand flux q_s, and the only parameters are those which are relevant for the magnitude of q_s according to the topography (Kroy et al. 2002a; Andreotti et al. 2002). Schematically, for a strong enough wind, deposition dominates if q approaches q_s (i.e $\partial_x q < 0$), else erosion occurs (i.e $\partial_x q > 0$). In all cases, there are different ways the grains can be put into movement. First, they can be dragged, lifted and accelerated by the excess shear stress exerted by the fluid on the surface. This corresponds to saltation. Second, they can be released by impacts of falling grains and crawl on the surface. This corresponds to reptation. These two transport modes are obviously related to one another, essentially because saltation implies an irregular hopping process through the retroaction of transported grains on wind velocity.

In this paper, we concentrate on the formation and the evolution of crescentic barchans dunes as a benchmark for a new model of sediment transport. Barchan dunes are isolated structures with horns extending downwind on both sides of an sand pile characterized by a slip face and a windward face (Fig. 1). Saltation and reptation are active on the windward face and the

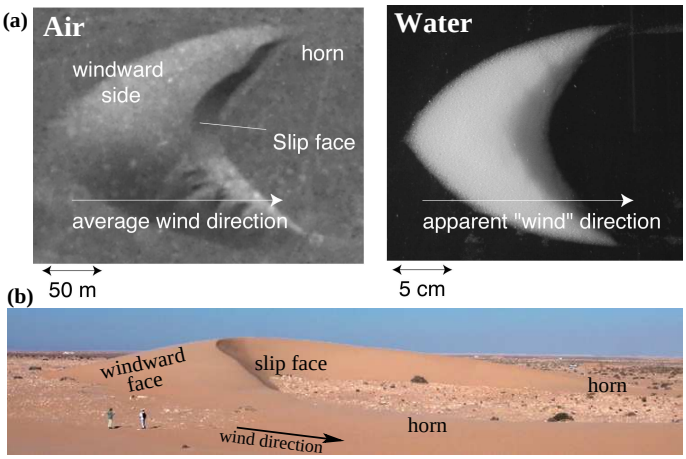

Figure 1: (a) Comparison between crescentic barchan dunes in air and water, in desert and laboratory experiments respectively (courtesy of *Physical Review Letters*, Hersen et al. (2002)). (b) Tranverse view of a barchan dune in Morocco (picture taken by B. Andreotti).

slope angle may vary from 10^o to 15^o; the slip face is not submitted to the dominant wind and its geometry is controlled by avalanches of grains reaching the dune crest. The angle of repose of the sand being approximately of 30^o, the dune profile is asymmetric in the direction of the wind. Barchans dunes have been observed in different geophysical environments on Earth (arid desert, icecap, deep water), on Mars, but also in laboratory experiments (Fig. 1). They are propagating downwind, and independent relationships can be deduced from their dimensions, volumes and velocities. Overall, the aim of this paper is to compare the predictions of our model with these relationships.

Following Nishimori and Ouchi (1993a) and Werner (1995), our numerical approach is dedicated to the analysis of emergence mechanisms in geomorphology. An emergence mechanism is met when one phenomenon leads to another, not in a direct cause/effect relationship, but in a manner that involves pattern of interactions between the elements of a system over time. In other words, an emergent macroscopic behavior can not be anticipated from the analysis of the constituent parts of the system alone, but can only result from their capacity to produce complex behaviours as a collective, through their mutual and repeated interactions. Such a complexity is an intrinsic property of cellular automata. Based on a discrete structure and a finite number of states at an elementary scale, cellular automata (CA) are systems that evolve on a network according to local interaction rules. These rules determine how each element responds to information transmitted from other elements along the network connections. Most of the time, these connections are simplified to include only interactions at a microscopic scale between nearest neighbors. CA are useful tools in physics, geophysics and biology to analyze pattern formation because their output match very well what we observe in nature without being dependent on a complete description of small scale processes. Thus, the origin of macroscopic behaviors as well as the emergence mechanism itself may be analyzed from a limited set of parameters. We exploit this property to implement a model conceptual enough to be applied on different types of geomorphological environments from aeolian dunes to river beds.

2 The model

Sediment transport is modelled by a Markov chain, a stochastic process characterized by a finite number of configurations evolving from one another according to a set of actions with different transition rates.

2.1 Length and time scales

A three-dimensional regular lattice models an interface between a turbulent fluid (air or water) and a layer of erodible sediment lying on a solid flat bedrock. This interface is subject to a so-called *fluid action* constant in magnitude and direction. An elementary cell has the shape of a parallelepiped, with 90^o angles, a square base of length l and a height h. We focus on sediment flux rather than on individual particle motions and h is therefore equal to l_d, the distance for a grain to accelerate up to the average fluid velocity:

$$l_d = \frac{\rho_s}{\rho_f} d \tag{2}$$

where ρ_s, ρ_f and d are the grain density, the fluid density and the characteristic length scale of a grain respectively. The choice for such a length scale is motivated by observations in desert area and laboratory experiments (Bagnold 1941; Hersen et al. 2002) as well as by analytical results together with numerical simulations (Kroy et al. 2002b; Andreotti et al. 2002). The aspect ratio $\eta = h/l$ corresponds to an upper limit of the slope angle θ upward in the direction of the flow ($\eta = \tan(\theta) < 1$). Finally, the characteristic time scale τ is determined from the dimensions of an elementary cell and an arbitrary volumic sediment flux Q (see Eq. 1):

$$\tau = \frac{lh}{Q}. \tag{3}$$

2.2 The discrete dynamic

Erosion does not affect the underlying solid bedrock and, at the bottom of the system, a layer of stable cells forms a flat surface where the transport of particles can create a topography. Then, we consider 4 states, 2 solid and 2 fluid. This is the minimum number of states necessary to implement retroaction mechanisms between a topography and a flow (Tab. 1). The two solid states, grains (G) and mobilized grains (M),

Action of fluid shear stress on topography	grains (G)
	mobilized grains (M)
Action of topography on fluid motions	fluid (F)
	Excess shear stress (S)

Table 1: 4 different states: 2 solid, 2 fluid. This is the minimum number of states to explore feedback mechanisms between circulation patterns and evolving topography.

allow to implement the action of fluid shear velocity on the surface. The two fluid states, fluid (F) and excess shear stress (S), allow to implement the action of topography on the flow pattern.

The indices (i, j, k), $i \in [1, L]$, $j \in [1, L]$, $k \in [1, H]$ label the Cartesian coordinates and the cell $c_{i,j,k}$ is either

- Grains (G): a G-cell represents a volume of sediment of uniform particle size.
- Mobilized Grains (M): a M-cell represents a volume of sediment transported by the fluid. Transportation of grains involves two transport modes related to one another: saltation and reptation. Here we do not differentiate between those modes.
- Fluid (F): a F-cell represents a volume of fluid where the velocity is under a threshold of erosion. Furthermore, particles can not be transported and F-cells are agent of deposition.
- Excess Shear Stress (S): a S-cell represents a volume of fluid where the shear stress exerted by the flow is above a threshold of erosion. S-cell are agent of erosion and transport by saltation and reptation.

N_G, N_M, N_F, N_S are the number of G-cells, M-cells, F-cells, S-cells respectively, and

$$N = N_G + N_M + N_F + N_S = L^2 H.$$

We do not consider long range interaction like other discrete approaches (Nishimori and Ouchi 1993b; Bishop et al. 2002), we only consider interactions between two neighboring cells with a common side (Von Neumann neighborhood, Fig. 2). These doublets of neighboring cells are noted $(c_{i,j,k}, c_{i\pm1,j,k})$, $(c_{i,j,k}, c_{i,j\pm1,k})$ and $(c_{i,j,k}, c_{i,j,k\pm1})$. As detailed below,

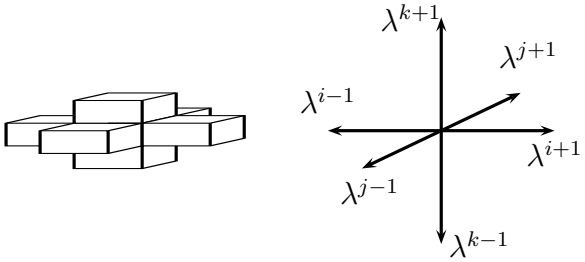

Figure 2: First neighbors in a regular rectangular parallelepiped mesh and the transition rates associated with a $c_{i,j,k}$-cell.

a cell may change states only if it shares an edge with a neighboring cell in a different state. In addition, we make a distinction between the orientation of the doublets according to gravity and the direction of the flow. This choice yields the lowest number of possible configurations and transitions while allowing for modelling of the physical processes involved in the formation of bedforms.

The whole process is defined in terms of a Poisson process with stationary transition rates between the various possible states of the doublets of neighboring cells. Given a transition from state u to v, the probability distribution of the waiting time until the next transition is an exponential distribution with rate parameter λ_u^v. Then the probability that a pair of neighboring cells in state u undergoes a transition toward the state v in the infinitesimal time interval dt is $\lambda_u^v dt$. The practical way we proceed in the numerical simulations is detailed in appendix. The main point is that at each iteration three random numbers determine the time step, the doublet which undergoes a transition and the transition kind itself. Therefore the model possesses the Markov property as the next configuration (i.e. the future) is independent of the previous configurations (i.e. the past), given the knowledge of the present configuration. This probabilistic approach and the physical processes represented by different set of transitions distinguish our model from classical CA (Narteau et al. 2001).

2.3 The physical processes

Each of the physical processes that we will now describe corresponds to a set of transitions. A transition of a given set cannot be considered in isolation because only combined and repeated actions are capable of reproducing these processes. For the same reason, transition rates are determined by reference to characteristic times representative of the given physical processes.

2.3.1 Fluid flow

At a given altitude above a flat surface, the velocity field might be considered constant in magnitude and direction, and the velocity profile is known to increase according to a logarithmic function (Landau and Lif-

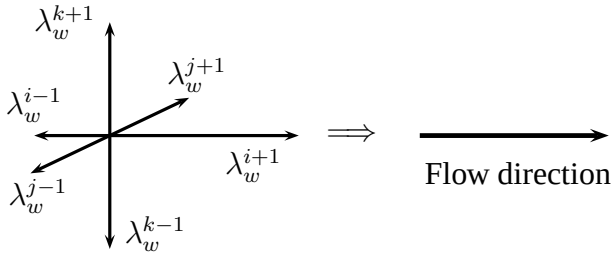

Figure 3: Transition rates of the permutation between a S-cell located in $c_{i,j,k}$ and a F-cell located in $c_{i\pm1,j,k}$, $c_{i,j\pm1,k}$, $c_{i,j,k\pm1}$.

shitz 1963). This is not the case above a rough surface, over which a flow might produce an highly turbulent circulation especially when it involves erosion, deposition and transport. Here, we adopt simplifying assumptions to limit the scope of the model on fluid velocity above topography.

As the streamlimes approach an obstacle, they converge and the velocity increases; after this obstacle, the streamlines diverge and the velocity decreases. Such observations are put into practical effect through the motions of S-cells in an ocean of F-cell by considering the following transitions:

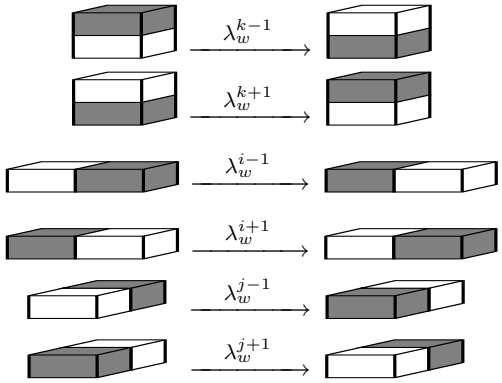

Each of these transition can be characterized by a vector according to the orientation of the doublet and the magnitude of the transition rate (Fig. 3). The resulting vector, i.e. the sum of the six vectors, determines the direction of the flow as well as the intensity of the turbulent diffusion. λ_w being an estimate of the turbulent diffusion, we take $\lambda_w^{j-1} = \lambda_w^{j+1} = \lambda_w^{k-1} = \lambda_w^{k+1} = \lambda_w$ and $\lambda_w^{i+1} > \lambda_w > \lambda_w^{i-1}$. As a consequence, the flow is going eastward (Fig. 3). On the other hand, the velocity of this flow cannot be determined only by the transition properties, but, as explained below, it can be approached through the proportion of S-cells in the fluid.

2.3.2 Erosion

Grains are lifted and dragged by the shear stress applied by the moving fluid and set in motions in the direction of the flow. This erosion process, which does not discriminate between saltation and reptation, involves two types of transition:

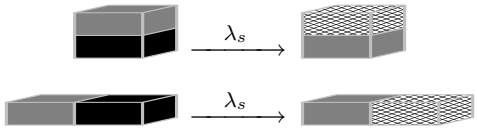

Practically, S-cells in contact with G-cells produce M-cells upward and in the direction of the flow. These transitions are the only source of transport in the model. Taking the sediment flux Q as a control parameter, the magnitude of the transition rate λ_s is derived directly from τ (see Eq. 3).

2.3.3 Transport

If the fluid velocity is high, grains already in motion can be transported upward and in the direction of the flow. Such a transportation involves two transitions based on the permutation of M-cells in contact with S-cells:

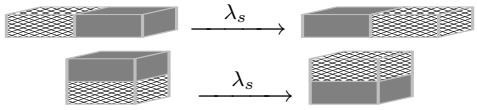

The magnitude of this sediment transport is proportional to Q and, by convention, the transition rates is taken equal to λ_s.

2.3.4 Deposition

When the fluid velocity is not high enough to maintain particles in suspension, deposition occurs. This deposition of fluid-borne grains is enhanced by topographic obstacles and occurs faster on slopes of existing structures. This process involves the following transitions

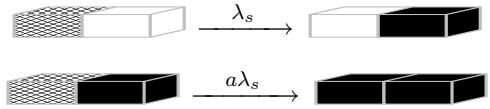

where G-cells are created from M-cells if they are not in contact with S-cells. $a > 1$ and, for the sake of simplicity, we assume that the deposition rate is equal to λ_s, the erosion rate.

2.3.5 Diffusion

Horizontal diffusion disperses the grains and flattens the topography. This process involve the following permutations between G-cells and F-cells:

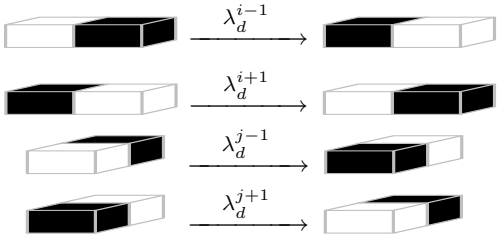

where $\lambda_d = \lambda_d^{i-1} = \lambda_d^{i+1} = \lambda_d^{j-1} = \lambda_d^{j+1}$ is the inverse of a characteristic time for diffusion.

l_d	$0.44\ m$
Θ	11.3^o
Q	$100\ m^2.yr^{-1}$
$\lambda_s\tau$	6
$\lambda_w\tau$	6
$\lambda_d\tau$	0.06
$\lambda_g\tau$	6000
a	10

Table 2: Parameters of the model and their values.

2.3.6 Gravity

Sand grains fall under their own weight and exert pressure on all the other grains. Gravity prevents further motions and leads to deposition. We attribute the following transition to these gravitational processes:

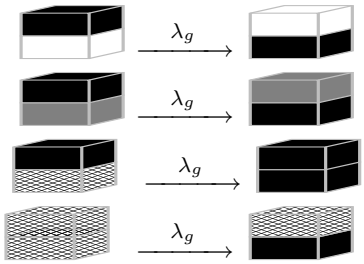

They include downward permutations between G-cells and fluid-states as well as depositions of M-cells located under solid-states. λ_g is determined from the Stokes velocity and it is generally few orders of magnitude larger than all the other transition rates.

3 Numerical simulations

The model involves 20 transitions characterized by a limited number of independent transition rates. Before we present the results of the numerical simulations, different aspects of the model can be addressed when looking at all the transitions together. First, the conservation of mass is ensured by the constant number of solid cells ($N_G + N_M = cte$). Second, S-cells are persistent in all transitions ($N_S = cte$) in such a way as to ensure the fluid forcing. As a consequence, we are dealing with an open system which relies on the balance between erosion and deposition to ensure the conservation of momentum at a macroscopic scale. For this reason, the proportion of S-cells in the fluid has to be low, $\beta = N_S/N_F \ll 1$, and the fluid velocity can only be derived from β.

Table 2 shows all the model parameters and their numerical values for all the simulations presented in this work. In this case $\tau \approx 3.5\ day$ and $l_d/\tau \approx 0.13\ m.day^{-1}$. Initial conditions and boundary conditions are essential aspects of the long-term development of topography and we focus here on two different set of conditions in order to analyze the evolution of some physical quantities as well as different properties of pattern formation.

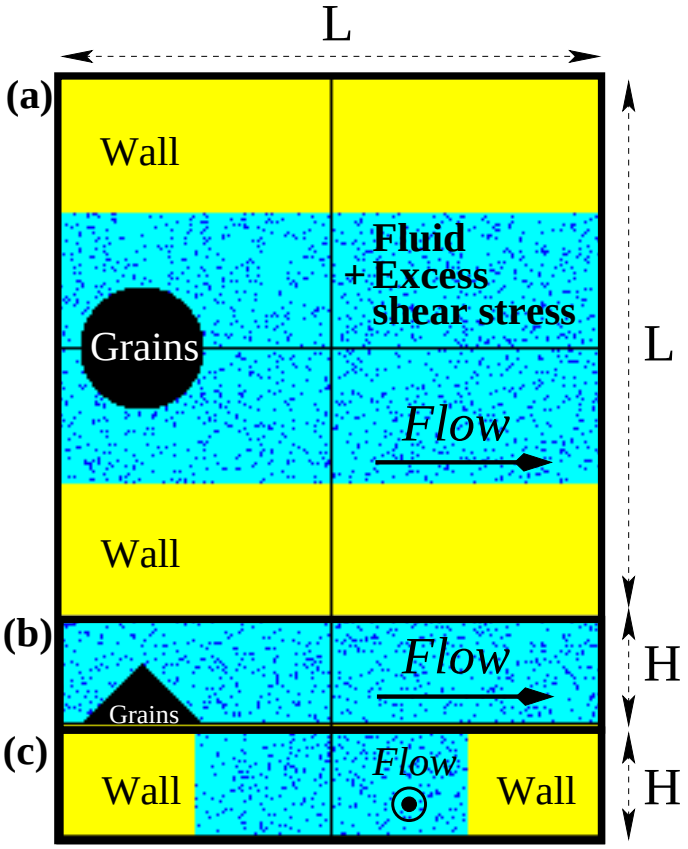

Figure 4: Model for a conical pile of sediment in a corridor. Three layer of cells are represented without the aspect ratio: (a) a horizontal layer just above the flat bedrock, (b) a vertical layer parallel to the flow, (c) a vertical layer perpendicular to the flow. In each figures, black lines indicate layer intersections.

3.1 Evolution of a conical bump

First we are interested in stationary patterns and we analyze the evolution of a conical bump of sediment in a corridor (Fig. 4): $L = 200$, $H = 40$, $\beta = 0.15$ and two walls facing each other form a corridor $L/2$ wide parallel to the flow; the cone has a base radius of 45 and a half summit angle equal to Θ. In addition, we consider asymmetric boundary conditions in the direction perpendicular to the flow in order to satisfy simultaneously mass conservation and a homogeneous injection of material. Practically, each G-cell ejected from the system in the direction of the flow is reinjected randomly through the opposite boundary.

Under such conditions, the distribution of S-cells rapidly changes on both sides of the obstacle as they abandon slopes oriented in the direction of the flow and accumulate on the slopes oriented against the direction of the flow. Where the density of S-cell increases, shear stress is higher and erosion and transport dominate (see the location of M-cells in Fig. 5). On opposite slopes, where the density of S-cell decreases, fluid velocity is lower and deposition is more likely to occur. Then a flux of sediment results from the motion of grains (i.e. M-cells) from one side to

another of the sediment pile and the symmetry of the cone shape is broken (Fig. 5). Interestingly, the slope is smaller on the face oriented against the direction of the flow than on the opposite face. The height of the cone varies and, where it is lower, particles propagate more rapidly in the direction of the flow. This produces horns of both sides on the cones (Fig. 5). As this evolution proceeds the structure moves in the direction of the flow and converges toward a stationary state which is commonly describes as a crescentic shape barchan dune.

Fig. 6 shows the evolution of the dimension of such a barchan dune over long time. Width, length and height reach a stable value despite important variations inherent to our discrete approach. Stronger fluctuations of the length result from unstable behaviors along the horns where the density of G-cells is lower. The emergence and persistence of a stationary crescentic shape (see contours in Fig. 6) demonstrate that erosion and deposition can balance each other under specific (unrealistic?) conditions. However, from a theoretical point of view, this is a chance to analyze different physical quantities under a statistically-stable regime.

As the flux of grains on the crest and in the horns stabilize as well, the barchan dune reaches a constant velocity of $v = 0.18\ l_d/\tau$ (Fig. 7). In more conventional units, $v = 8.25\ m.yr^{-1}$ for an height of $H \approx 10.2\ m$. Over short time, the barchan tends to accelerate with respect to a loss of volume associated to a redistribution of grains in the entire system (see contour plots in Fig. 7). This relationship between the volume of the dune and its velocity is of primary importance in dune fields because it results inevitably in dune interaction patterns.

3.2 Evolution of randomly distributed sediment

We are now interested by these patterns of interaction between dunes and we analyze the evolution of homogeneously distributed sediment in a corridor (Fig. 8). As before, $L = 200$, $H = 40$, $\beta = 0.15$, and two walls facing each other form a corridor $L/2$ wide parallel to the flow; on two layers just above the flat bedrock, G-cells are randomly distributed with the probability $p = 0.65$. In addition we consider periodic boundary conditions.

Over short time, grains form clusters which deform in the direction of the flow (Fig. 9). These clusters coalesce to produce elongated structures that start to modify significantly the density of S-cells in their neighborhood. All these structures propagates at different velocity according to their geometry and volume. Smaller structures being faster, they merge with larger ones which in turn decelerate. Thus, a set of crescentic barchan dunes emerge. Each of them is similar to the one describe in the previous section but

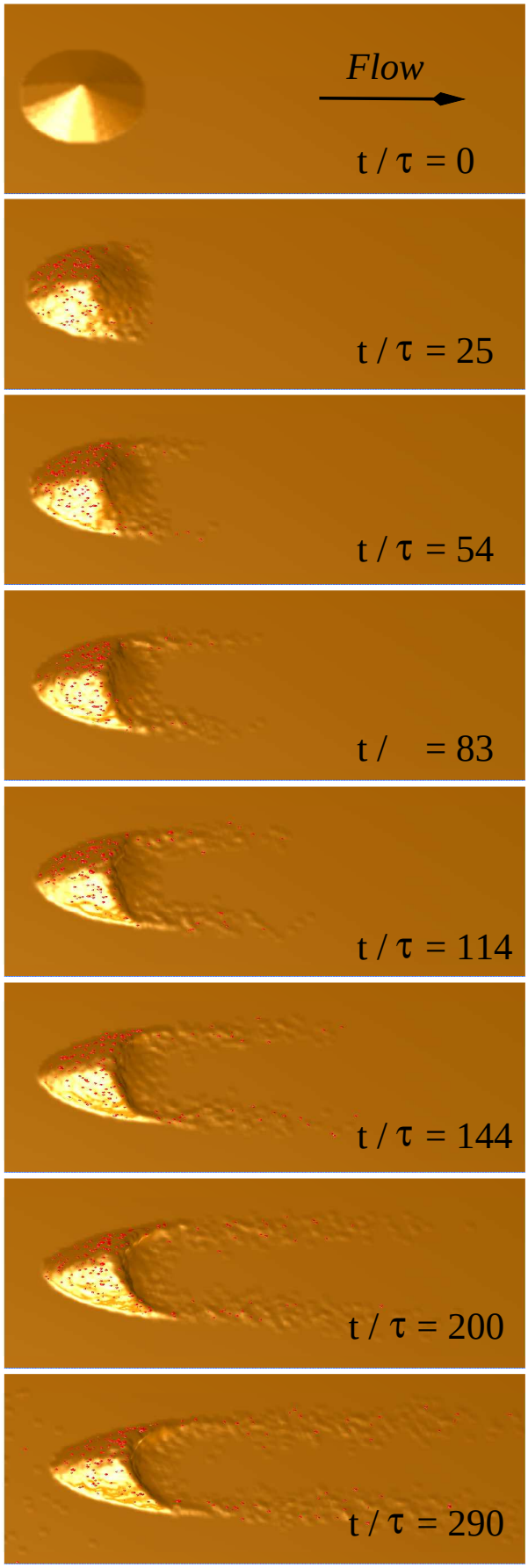

Figure 5: Evolution of a conical bump over short time. Each figure is obtained by smoothing the topography obtained from G-cells. Dots are the M-cells. They are essentially located on the slope oriented against the direction of the flow.

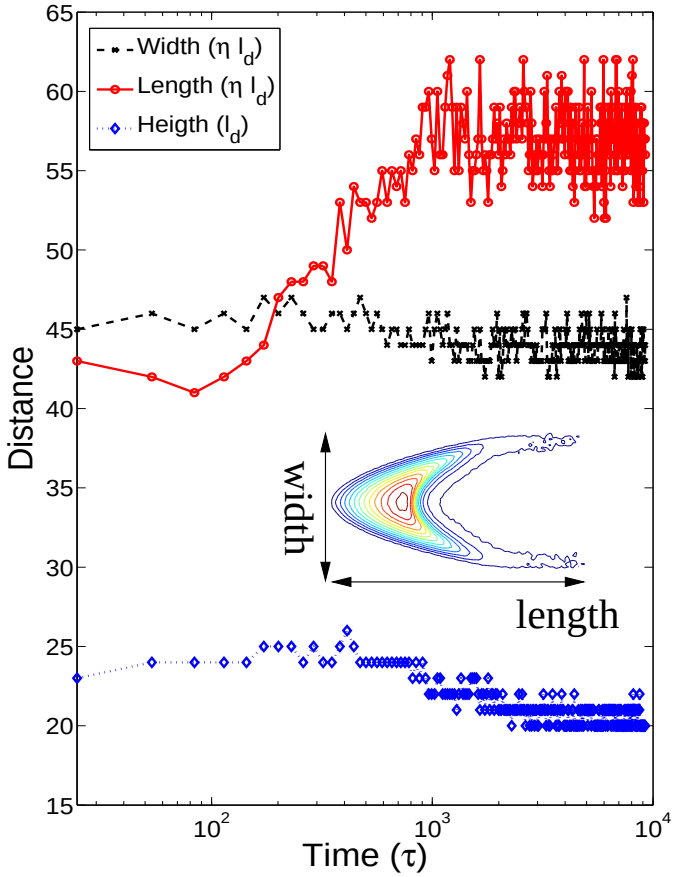

Figure 6: Evolution of the width, the length and the height of the conical bump in a logarithmic scale over long time. Note that the dimensions of the barchan stabilize. The inset shows the stationary crescentic shape where the height between level-lines is $1.5\ l_d$.

their interaction make their respective evolution much more complicated. Finally, in this particular simulation, the last configuration of dunes (i.e $t/\tau = 1187$) is not subject to strong changes and the set of dunes of similar size is extremely resilient. The main reason for such a behavior is the small size of the system and the periodic boundary conditions which impose that all dunes propagate within their own shadow.

Nevertheless, the formation and the evolution of dune fields provides the opportunity to compare model predictions to field measurements. To reduce significantly finite size effect, model statistics have been computed on much larger systems with $L = 10^3$ and $H = 10^2$, with similar initial conditions than in Fig. 8 but without walls.

Structural properties are estimated from the output of the model at one point in time. For barchans observed in arid deserts and in the numerical simulations, Fig. 10 shows the relationships between width and length, Fig. 11 shows the relationships between width and height. These two independent morphological relationships are well fit by lines and there are good agreements between synthetic data and field measurements.

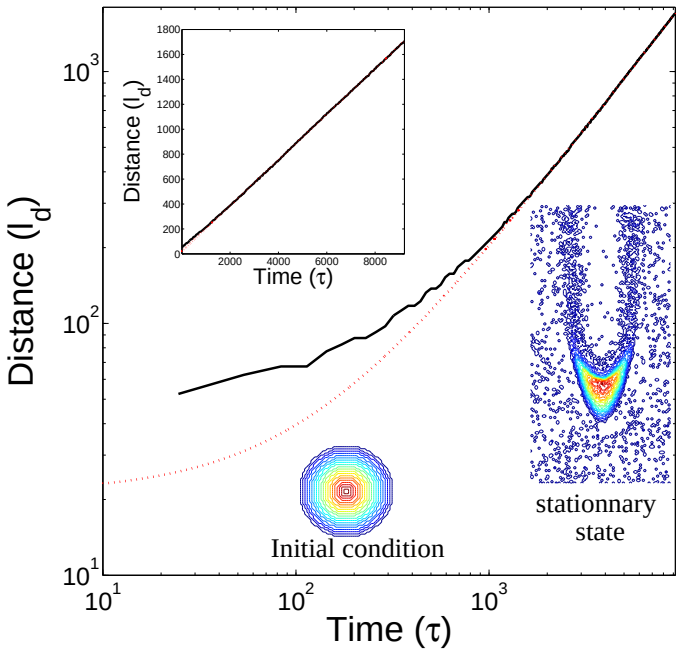

Figure 7: Position of the sediment pile with respect to time (solid line) in (a) linear and (b) logarithmic scales. Over long time, the velocity of the barchan is constant (dotted lines: $y \sim 0.03x$). Over short time, the sediment pile accelerates during the transition from a conical shape to a barchan shape. It corresponds to a loss of volume associated with the redistribution of grain escaping from the horns (see contour plots).

In the model, the dune measured in Figs. 10 and 11 are studied over long time ($\Delta t/\tau = 335$) to approximate their average velocity v. Fig. 12 shows the relationship between height and velocity for numerical and observed barchan dunes. One more time, the output of the model and the natural data are in good agreement and it is possible to fit both set of measurements with

$$v = \frac{Q_1}{H + H0}.$$

where Q_1 is a volumic sand flux and H_0 a characteristic height. Here, we have $Q_1 = 7\ l_d^2.\tau^{-1}$ and $H_0 = 4.0\ l_d$. In more conventional units, $Q_1 = 140\ m^2.yr^{-1}$ and $H_0 = 1.7\ m$.

4 Discussion and Conclusion

Under specific conditions, our model reproduces crescentic barchan dune patterns that compare well with observations. Firm morphological and velocity constraints are satisfied and validate the predictions of our model based on short scales interactions. Flux measurements have now to be investigate as we are aware that a full understanding of dune dynamics should include estimation of transport capacity on different parts of the topography.

In the last decades, different scientists have explored a variety of CA approach in order to model

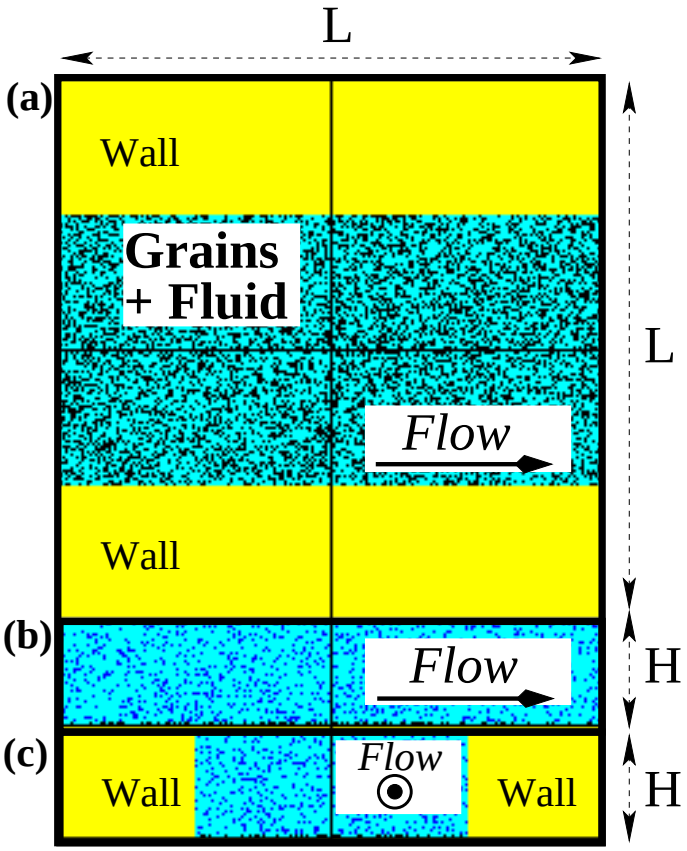

Figure 8: Model for randomly distributed sediment in a corridor. Three layer of cells are represented without aspect ratio: (a) a horizontal layer just above the flat bedrock where G-cells are randomly distributed with the probability $p = 0.65$, (b) a vertical layer parallel to the flow, (c) a vertical layer perpendicular to the flow. In each figures, black lines indicate layer intersections.

dune patterns under dry conditions (Nishimori and Ouchi 1993a; Werner 1995; Nishimori et al. 1999). Models are based on a characteristic saltation length and on rules involving long range interactions. In all cases, despite a stochastic ingredient, the trajectory of an elementary volume of grains is given from the present configuration of cells, and the rules do not allow to dissociate between transport and erosion-deposition processes. In addition, there is no treatment of aerodynamics effect. Here, we present a CA approach in which erosion and deposition locally depend on flow patterns that are affected in turn by the surface profile. Such an innovation will allow to concentrate on relationships between shear stress and topography and to characterize turbulent flow patterns on an evolving surface (Wiggs 2001). This goal can be achieved by considering more realistic small scale interactions for the dynamic of S-cells.

In this preliminary work, the transport is simplified to the extreme in order to concentrate on the first requirement of this kind of models, the formation and the development of realistic structural patterns. Nevertheless, we have shown that anisotropic motions

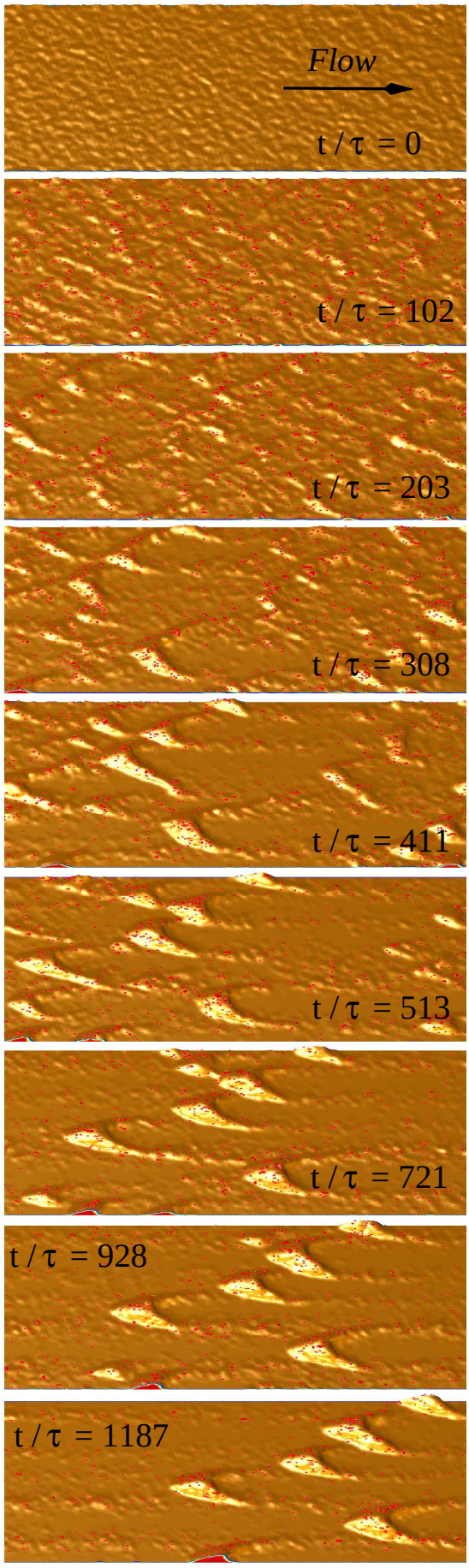

Figure 9: Evolution of homogeneously distributed sediment over long time. Figure are obtained by smoothing the topography obtained from G-cells. Dots are the M-cells.

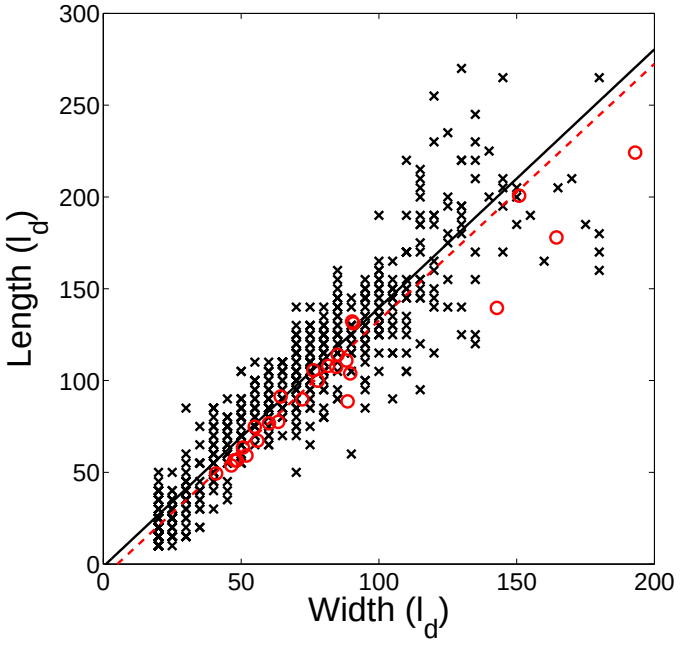

Figure 10: Relationships between barchan width and length in arid deserts (gray ∘) and in the model (black **x**). Field measurements are averaged by ranges of height. Predictions of the model represent individual dune. The solid line ($y = 1.40x - 1.27$) and the dashed line ($y = 1.39x - 6.5$) fit the synthetic and the real data respectively (Andreotti et al. (2002) compiled observations from Finkel (1959), Hastenrath (1967), Hastenrath (1987)).

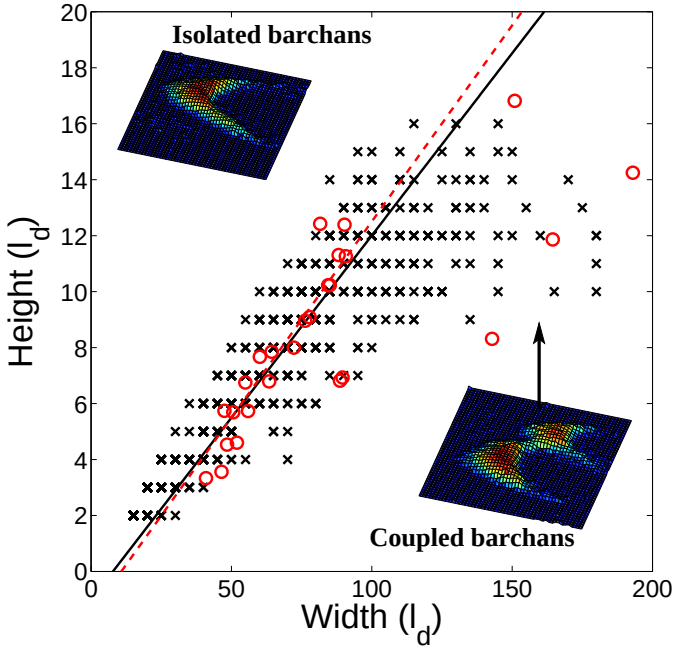

Figure 11: Relationships between barchan width and height in arid deserts (gray ∘) and in the model (black **x**). Field measurements are averaged by ranges of height. Predictions of the model represent individual dune. The solid line ($y = 0.13x - 1.01$) and dashed line ($y = 0.14x - 2.1$) fit the real and the synthetic data respectively (Andreotti et al. (2002) compiled observations from Finkel (1959), Hastenrath (1967), Hastenrath (1987)).

of S-cells and an evolving topography are enough to reproduce the existence of a shadow zone downwind, the concentration of shear stress on the windward face, and, as said above, dynamical properties of barchan dune fields. Such qualitative features of physical fluid behaviour have now to be replaced by more quantitative analysis. In the field of turbulence, it is common to analyze fluid dynamics from particle collisions (Frisch et al. 1986). This lattice gas method converts discrete motions into physically meaningful quantities and dispenses with the need to solve the Navier-Stokes equations. The discrete nature of our system offers the opportunity to develop such a lattice gas method based, as the actual model, on short range interactions between a finite number of states. As a result of a more generalized set of transitions (i.e. erosion, deposition and transport occurring in all direction), realistic structures and fluid circulations might appear together.

This model has been developed to be applied to different type of systems, in particular for the analysis of bedform. Fig. 13 shows a snapshot of a model simulation similar to the one presented on Fig. 8 but with 10 times more sediment (i.e. G-cells). There is no individual structures and larger structures perpendicular to the flow develop. These structures exhibit similarities with bars in river. The bar dynamic and the subsequent morphology of river will be studied by going further in this direction.

More generally, our model can also be adapted to different types of geometry and boundary conditions. In order to compare the predictions of the model with classical observations of physical geography, it is possible to concentrate on

1. the impact of the variability of wind direction as well as the impact of sediment availability (compare Figs.9 and 13). The primary objective will be to reproduce different types of dune (e.g. linear dunes, star dunes) and to locate them in a phase diagram. Another objective could be to estimate the orientation of dune crests according to the magnitude of the wind fluctuation in order to analyze dune attractor trajectories (Anderson 1996) and defect behaviors (Werner and Kocurek 1997).

2. the role of vegetation on erosion and deposition rates, and the effect of a vegetal cover on structural and dynamical dune patterns.

3. the interaction between dune patterns and structures related to human activity (e.g. accumulation of sand around constructions).

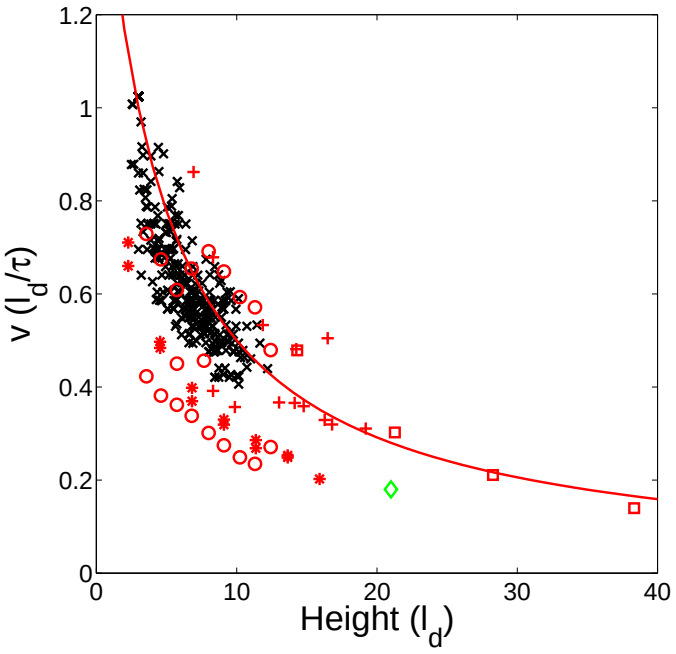

Figure 12: Relationships between barchan width and velocity in arid deserts (gray symbols), and in the model (black **x**). Field measurements are averaged by ranges of height. Predictions of the model represent individual dune. The line fits the synthetic data and follows $v = 1.25/(H + 5.5)$. The diamond symbol is for the barchan dune shown in Fig. 5. (Andreotti et al. (2002) compiled observations from Finkel (1959) ($*$), Hastenrath (1967) ($\circ$), Hastenrath (1987) ($\circ$), Slattery (1990) (square), and Long and Sharp (1964) ($+$)).

Note that in all cases there are reciprocal applications in the analysis of bedforms underwater.

In geomorphology, as in many domains in science, description in terms of differential equations have limits that can be related to a lack of theoretical backgrounds, the role of heterogeneities and numerical limitations. Then, CA approach can be described as an alternative which focus on self organization and the emergence of structure without taking into account all the diversity of the small scale physical processes. Trough our model, we try to provide a link between classical CA methods and continuum mechanics in such the way that we will be able to constrain structural complexity of geophysical system by a set of well-defined physical quantities. We believe that the discontinuous nature of our model and the feedback mechanisms between different types of states will allow this system to move between different basins of attractions and therefore capture in detail some of the more distinctive features of the evolution of bedforms.

Acknowledgments

We thank B. Andreotti and P. Claudin for helpful discussions, figures and fields measurements. A preliminary work of E. Sepulveda was of great help. This work was supported by E2C2, a Specific Targeted Research Project of the European Community. In the I.P.G.P., Clément Narteau benefit from a Marie Curie reintegration grant 510640-EVOROCK of the European Community.

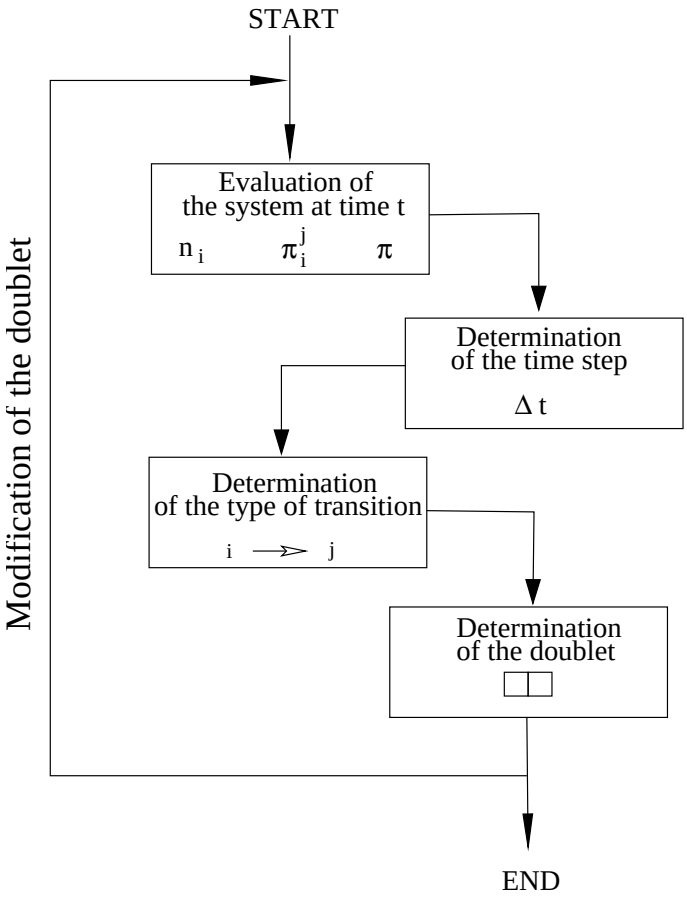

Figure 14: The algorithm of the model. n_i is the number of doublets in state i, π_i^j the rate parameter of the transition of doublet from state i to j, and π the rate parameter of the entire system. To respect the Markov property, only one doublet of cells is changed at each iteration. The time step, the transition type and the doublet are successively chosen according to the present configuration of the system and three random numbers.

Appendix

Here we present in more detail how we combine a Poisson process with a Markov chain with stationary transition rates. The algorithm is schematically describe in Fig. 14.

As said above, we consider only first neighbors interactions and transition of doublets of cells in a D-dimensional parallelepipedic mesh. Overall, all transitions and doublets are independent of one another. Each cell can be in one of N_s states. Then, the number of different doublets is

$$N_d = DN_s^2$$

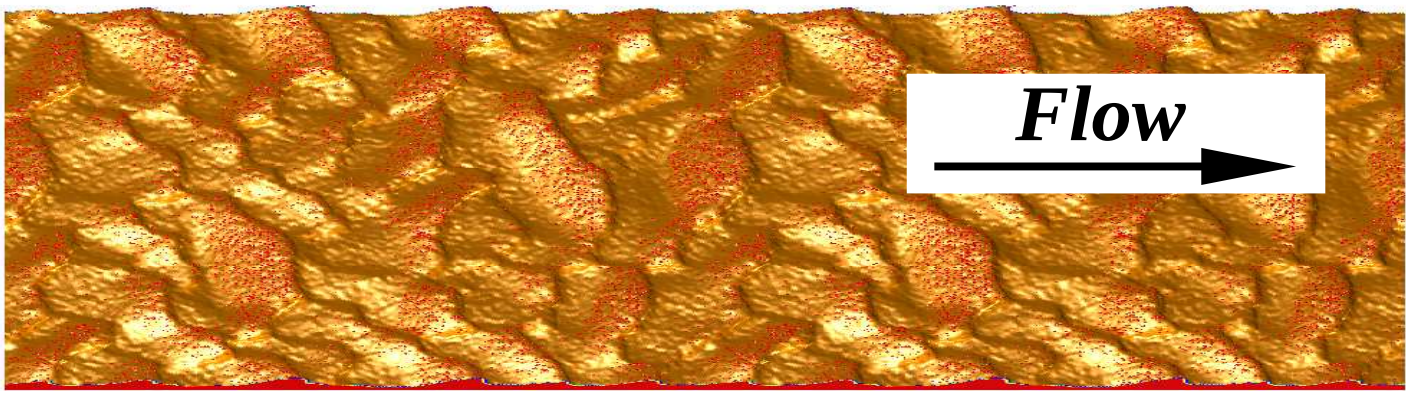

Figure 13: A snapshot of a model simulation with more sediment. This figure is obtained by smoothing the topography obtained from G-cells. Dots are the M-cells.

and the number of doublets in a $L \times W \times H$ mesh is

$$N = HL(W-1) + WH(L-1) + LW(H-1)$$

.

For a given configuration at time t, we first determine n_i the number of doublets in state i:

$$N = \sum_{i=1}^{N_d} n_i.$$

A transition of doublet from state i to j is modelled by a Poisson process with a rate parameter λ_i^j. Then, the occurrence of such a transition in a population of doublets i follows also a Poisson process with rate parameter

$$\pi_i^j = n_i \lambda_i^j.$$

Generalized to all doublets and transitions, the total transition rate in the entire system is

$$\pi = \sum_{i=1}^{N_d} \sum_{j=1}^{N_d} \pi_i^j.$$

At each iteration, only one doublet makes a transition from one state to another. The time step Δt is therefore variable, randomly chosen according to the magnitude of π. Practically, we draw at random a value R_1 between 0 and 1, and we consider that the characteristic time necessary for a transition to occur is

$$\Delta t = -\frac{1}{\pi} \ln(R_1).$$

During this time step, the type of transition is also randomly chosen with respect to a weighted probability determined from the π_i^j-values

$$P_i^j = \frac{\pi_i^j}{\pi}.$$

Numerically, we define a cumulative step function ranging from 0 to 1, where jumps are proportional to the P_i^j-values. Then we draw at random a value R_2 between 0 and 1. This value falls within a jump of the cumulative step function which determines in turn the type of transition to occur. Thus, transition with the highest rates have more chance to be selected but transitions with small rates may also occur. These *rare* events are an essential ingredient of the modelling developed in this paper.

Finally, when the transition from i to j is selected, we draw at random an integer between 1 and n_i. Thus we identify the doublet which makes a transition.

REFERENCES

Anderson, R. S. (1996). The attraction of sand dunes. *Nature 379*, 24–25.

Andreotti, B., P. Claudin, and S. Douady (2002). Selection of dune shapes and velocities: Part 1: Dynamics of sand, wind and barchans. *European Physical Journal B 28*(3), 321–339.

Bagnold, R. A. (1941). *The physics of blown sand and desert dunes.* London: Methuen.

Bishop, S. R., H. Momiji, R. Carretero-gonzalez, and A. Warren (2002). Modelling desert dune fields based on discrete dynamics. *Discrete Dynamics in Nature and Society 7*(1), 7–17.

Finkel, H. J. (1959). The barchans of southern Peru. *Journal of Geology 67*, 614–647.

Frisch, U., B. Hasslacher, and Y. Pomeau (1986). Lattice-gas automata for the navier-stokes equation. *Physical Review Letters 56*(14), 1505–1508.

Hastenrath, S. (1967). The barchans of the Arequipa region, southern Peru. *Zeitschrift für Geomorphologie 11*, 300–331.

Hastenrath, S. (1987). The barchan dunes of southern Peru revisited. *Zeitschrift für Geomorphologie 31-2*, 167–178.

Hersen, P., S. Douady, and B. Andreotti (2002). Relevant length scale of barchan dunes. *Physical Review Letters 89*(26).

Hunt, J. C. R., S. Leibovich, and K. J. Richards (1988). Turbulent wind flow over smooth hills. *Q. J. R. Meteorol. Soc. 114*, 1435–1470.

Jackson, P. S. and J. C. R. Hunt (1975). Turbulent wind flow over a low hill. *Q. J. R. Meteorol. Soc. 101*, 929.

Kroy, K., G. Sauermann, and H. J. Herrmann (2002a). Minimal model for aeolian sand dunes. *Physical Review E 66*(031302).

Kroy, K., G. Sauermann, and H. J. Herrmann (2002b). Minimal model for sand dunes. *Physical Review Letters 88*(054301).

Lancaster, N. (1995). *Geomorphology of desert dunes*. London: Routledge.

Landau, L. D. and E. M. Lifshitz (1963). *Fluid Mechanics, Course of Theoritical Physics Vol. 6*. Pergamon Press, London.

Long, J. T. and R. P. Sharp (1964). Barchan dune movement in Imperial Valley. *Geophys. Soc. America 75*, 149–169.

Narteau, C. and Le Mouël, J. L. and Poirier, J. P. and Sepúlveda, E. and Shnirman, M. G. (2001). On a small scale roughness of the core-mantle boundary. *Phys. Earth Planet. Int. 191*, 49–61.

Nishimori, H. and N. Ouchi (1993a). Computational models for sand ripple and sand dune formation. *Int. J. of Mod. Phys. B 7*(9 & 10), 2025–2034.

Nishimori, H. and N. Ouchi (1993b). Formation of ripple patterns and dunes by wind-blown sand. *Phys. Rev. Lett. 71*(1), 197.

Nishimori, H., M. Yamasaki, and K. H. Andersen (1999). A simple model for the various pattern dynamics of dunes. *Int. J. of Modern Physics B 12*, 257–272.

Pye, K. and H. Tsoar (1990). *Aeolian sand and sand dunes*. London: Unwin Hyman.

Slattery, M. C. (1990). Barchan migration on the kuiseb river delta. *S. Afr. Geogr. J. 72*, 5–10.

Weng, W. S., J. C. R. Hunt, D. J. Carruthers, A. Warren, G. F. S. Wiggs, I. Livingstone, and I. Castro (1991). Air flow and sand transport over sand–dunes. *Acta Mechanica (Suppl.) 2*, 1–22.

Werner, B. T. (1995). Eolian dunes: Computer simulations and attractor interpretation. *Geology 23*, 1107.

Werner, B. T. and G. Kocurek (1997). Bed-from dynamics: Does the tail wag the dog? *Geology 25*, 771–774.

Wiggs, G. F. S. (2001). Desert dune processes and dynamics. *Progress in Physical Geography 25*, 53–79.